Available online at www.sciencedirect.com
ScienceDirect
International Journal of Mass Spectrometry 268 (2007) 8–15
International Journal of Mass Spectrometry
www.elsevier.com/locate/ijms

Evolution of the electronic structure and properties of neutral and charged cobalt-doped aluminum clusters

Ling Guo

School of Chemistry and Material Science, Shanxi Normal University, Linfen 041004, China

Received 18 May 2007; received in revised form 31 July 2007; accepted 1 August 2007
Available online 7 August 2007

Abstract

Structural and electronic properties of neutral and ionic Al_nCo ($n = 8$–17) clusters have been investigated by performing density-functional theory calculations within the effective core potential level. The total energies of these clusters are then used to study the evolution of their binding energy, relative stability, ionization potential, and vertical and adiabatic electron affinities as a function of size. Unlike the alkali atom-doped aluminum clusters in the same size range, the most cobalt atom resides inside the aluminum cluster cage except for $Al_{12}Co$, $Al_{13}Co$, $Al_{11}Co^-$, $Al_{11}Co^+$ and $Al_{13}Co^+$ clusters. Furthermore, the 3d and 4s energy levels of Co hybridize with the valence electrons of Al causing a redistribution of the molecular orbital energy levels of the Al_n clusters. The binding energy evolves monotonically with size, but $Al_{13}Co$, $Al_{13}Co^-$ and $Al_{13}Co^+$ exhibit greater stability than their neighbors, which is consistent with the large HOMO–LUMO gaps. The calculated results agree reasonable with all available experimental data on ionization energies and electron affinities.

PACS: 36.40.−c; 61.46.+w; 71.15.Mb

Keywords: Cobalt-doped aluminum cluster; Density-functional theory; Stability

1. Introduction

Bulk phase bimetallic systems provide a matter of increasing interest in pure and applied materials sciences and traditional fields of physics and chemistry [1–6]. In catalytic chemistry and chemical engineering, real catalysts mainly consist of a heterometallic or bimetallic system, which can profoundly enhance reactivity and selectivity [7]. Thus, to get a deeper understanding of the microscopic behavior of these species, the study of bimetallic or so-called alloy clusters provides a suitable tool, since cluster science enables one to investigate chemical and physical properties starting from a single atom or molecule toward bulk phase as a function of size. Therefore, in the last decades a number of studies of bimetallic clusters and diatomic molecules have been performed [8–12].

Among the candidate systems to have been considered, the bimetallic aluminum cobalt clusters have been the topic some experimental and theoretical studies [13–17]. Several years ago, Nonose et al. [13] performed chemisorptions reactivity studies of neutral Al_nCo_m ($n > m$) and Co_nAl_m ($n > m$) clusters toward H_2 using a fast flow reactors. In that study, they found that the doping of Co_n clusters with only one Al atom reveals a remarkable increase of hydrogen chemisorptions rates compared to pure Co_n clusters. On the other hand, pure Al_n clusters do not adsorb hydrogen, which is comparable to Al bulk phase behavior [14]. Knickelbein and coworkers [15,16] succeeded in a comprehensive investigation of the size dependence of ionization energies of these clusters. These IE studies show that the electronic shell structure of Al_nCo and Al_nCo_2 clusters remains similar to that of pure Al_n clusters. Morse and co-workers [17] have performed resonant two-photon ionization spectroscopy on small diatomic AlCo aluminides. Pramann and co-workers [18] have measured the photoelectron spectra of small mass-selected aluminum-rich Al_nCo^- ($n = 8$–17) and cobalt-rich $Co_nAl_m^-$ clusters ($n = 6$, 8, 10; $m = 1$, 2) are measured at photon energies of 3.49 eV with the aid of a magnetic bottle photoelectron spectrometer.

In the present paper, to understand the anomalous behavior of the mass ion intensity in Al_nCo clusters, we have calculated the equilibrium geometries and total energies of neutral and ionic Al_nCo ($n = 8$–17) clusters using density-functional theory. We show that unlike the alkali atoms [19], cobalt prefers to occupy

E-mail address: gl-guoling@163.com.

1387-3806/$ – see front matter © 2007 Elsevier B.V. All rights reserved.
doi:10.1016/j.ijms.2007.08.001

internal sites in the aluminum clusters. This is because the size of the cobalt atom is smaller than that of aluminum. Second, the large ionization energy of Co (7.91 eV) makes it energetically unfavorable to transfer its outermost s electron to the Al_n cage and thus does not form an ionic bond between Al and Co. We have also calculated vertical and adiabatic detachment energies of Al_nCo^- clusters as well as the vertical and adiabatic ionization energies of Al_nCo clusters. The calculated electron affinities of these clusters agree very well with experiment proving indirect evidence of the accuracy of the computed geometries. In the following, we provide a brief outline of our computational procedure. A discussion of our results and a summary are given in Sections 3 and 4.

2. Theoretical procedure

In the present study, Al_nCo (n = 8–17) clusters have been investigated theoretically by performing density-functional theory calculations [20]. The exchange and correlation potential contributions have been considered at B3LYP level [21]. The compact effective potential (CEP) basis functions with ECP triple-split basis, namely, CEP-121G, [22–24] have been used in the calculations. The exchange term of B3LYP consists of hybrid Hartree–Fock (HF) and local spin density (LSD) exchange functions with Becke's gradient correlation to LSD exchange [25]. The correlation term of B3LYP consists of the Vosko, Wilk, and Nusair (VWN3) local correlation functional [26] and Lee, Yang, and Parr (LYP) correlation functional [27]. The BLYP method gives a better improvement over the SCF-HF results. Its predictions are in qualitative agreement with the experiment. In general, the DFT method overestimates the binding energies, and it gives shorter bond lengths than the experimental values. However, the optimized structures of Al_nCo (n = 8–17) clusters predicted at B3LYP level are in reasonable agreement with the experiment [28,29].

CEP-121G basis functions are becoming widely used in quantum chemistry, particularly in the study of compounds containing heavy elements [22–24]. The CEP basis sets have been used to calculate the equilibrium structures and spectroscopic properties of several small molecules [22]. The standard basis set of CEP theory was consistent for the entire series not only within the lanthanide series but also with the second- and third-row metals. The quality of the CEP-121G basis set does not degrade when going from the second to the third row of the periodic table. In the present calculations, CEP-1-21G basis set and the number of primitive Gaussians used in CEP-121G vary from atom to atom, depending on the valence structure of atoms considered. In the present paper, the optimized ground-state structures, electronic properties, and vibrational spectra of Al_nCo (n = 8–14) clusters have been calculated. All calculations have been done with the Gaussian 03 program [30]. Since one does not know a prior the spin multiplicity of the clusters, the above calculations are repeated for different spin configurations to obtain the lowest energy structure. We examined spin multiplicities of 1 and 3 for even-electron clusters and 2 and 4 for odd-electron clusters.

3. Results and discussion

3.1. Structural properties

The starting point in any description of cluster properties is its geometrical structure. Unfortunately, there is no experimental technique that can provide direct information on cluster geometry. The clusters are too large for spectroscopic techniques and too small for diffraction techniques to be of much use. In direct information on cluster geometries can be obtained by studying their reaction with reagent molecules [31], but their interpretation is plagued by assumptions and uncertainties. Raman spectroscopy [32] on matrix-isolated clusters has been recently used to study cluster geometries, but the effect of the matrix on the cluster geometry remains a nagging concern.

The only method that enables determination of cluster geometries at present is, thus, based on theoretical calculations. Unfortunately, the calculated geometries depend on the level of the theory. The better the theory, the smaller the size of the cluster it can handle. Simpler theories based on empirical schemes and model potentials can provide geometries of large clusters, but their accuracy remains questionable. The correctness of the geometries determined theoretically can only be established by comparing calculated properties of these clusters with experiment. We believe that we have identified the equilibrium geometries of cobalt-doped aluminum clusters containing up to 15 atoms correctly. This belief is based on our ability to explain the mass ion intensity, vertical and adiabatic electron affinities for all clusters studied consistently and quantitatively.

Fig. 1 presents the equilibrium geometries of Al_nCo (n = 8–17) clusters in neutral and ionic configurations, respectively. Note that in most clusters Co resides inside the Al_n cage except for $Al_{12}Co$, $Al_{13}Co$, $Al_{11}Co^-$, $Al_{11}Co^+$ and $Al_{13}Co^+$ clusters. In Table 1, we list the total energies of optimized Al_nCo, Al_nCo^- and Al_nCo^+ clusters.

Unlike in the bulk where the nearest-neighbor distance is well defined, the lack of a perfect structural symmetry in clusters makes it difficult to assign a unique nearest neighbor distance for each cluster. We define an atom to be counted as a nearest neighbor if its distances are less than 3.2 Å. This cutoff is arrived at by examining all the interatomic distances in the clusters studied and by noting that there is a distances gap in these distances beyond 3.2 Å. In Al_8Co to $Al_{17}Co$, the nearest-neighbor distances lie in the range 2.5369–3.1496 Å, 2.3959–3.0509 Å, 2.5318–2.9892 Å, 2.4270–3.1701 Å, 2.4930–3.1794 Å, 2.4660–3.1237 Å, 2.4377–2.9948 Å, 2.4117–3.1488 Å, 2.4803–3.1641 Å, and 2.4299–3.1860 Å, respectively. In Fig. 1, all bonds having lengths of 3.2 Å or less are connected.

In order to study the evolution of the nearest-neighbor distance, we have calculated the average nearest-neighbor distance by using the following expression:

$$\langle R \rangle = \frac{1}{n_b} \sum_{ij} R_{ij} \quad (1)$$

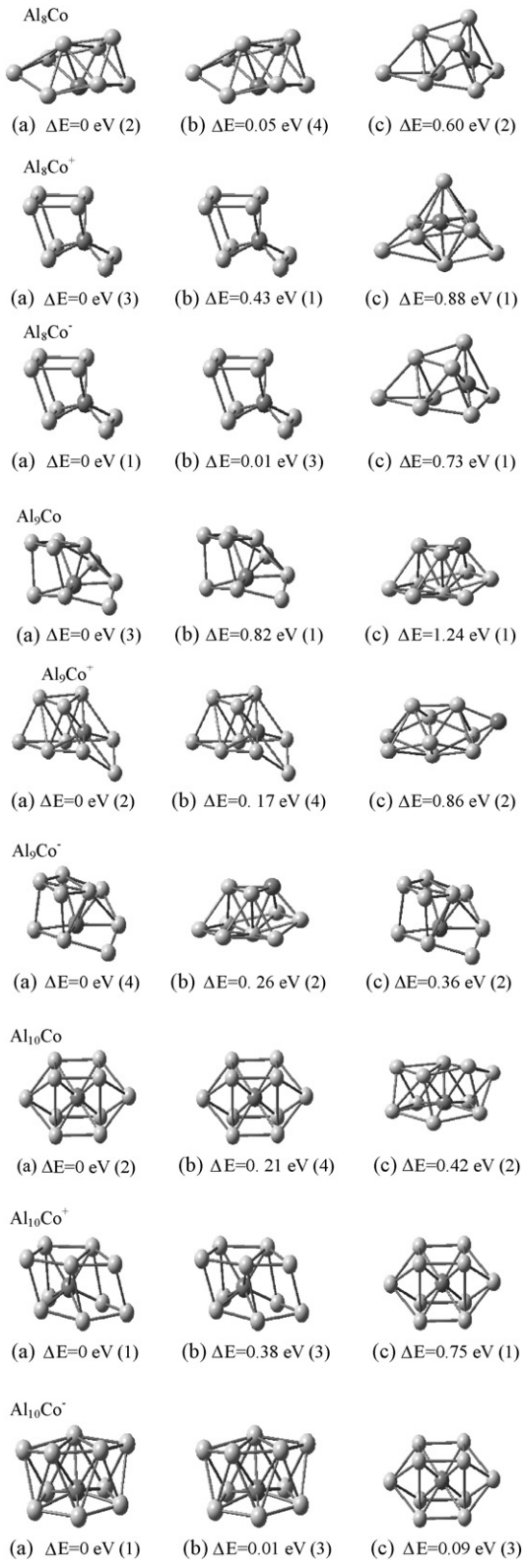

Fig. 1. The lowest-energy and low-lying structures of neutral, cationic and anionic Al_nCo ($n = 8$–17) clusters. The differences of total energies of an isomer from the most favorable isomer are given below the structure for each size. The values in the parentheses are the multiplicity of each size.

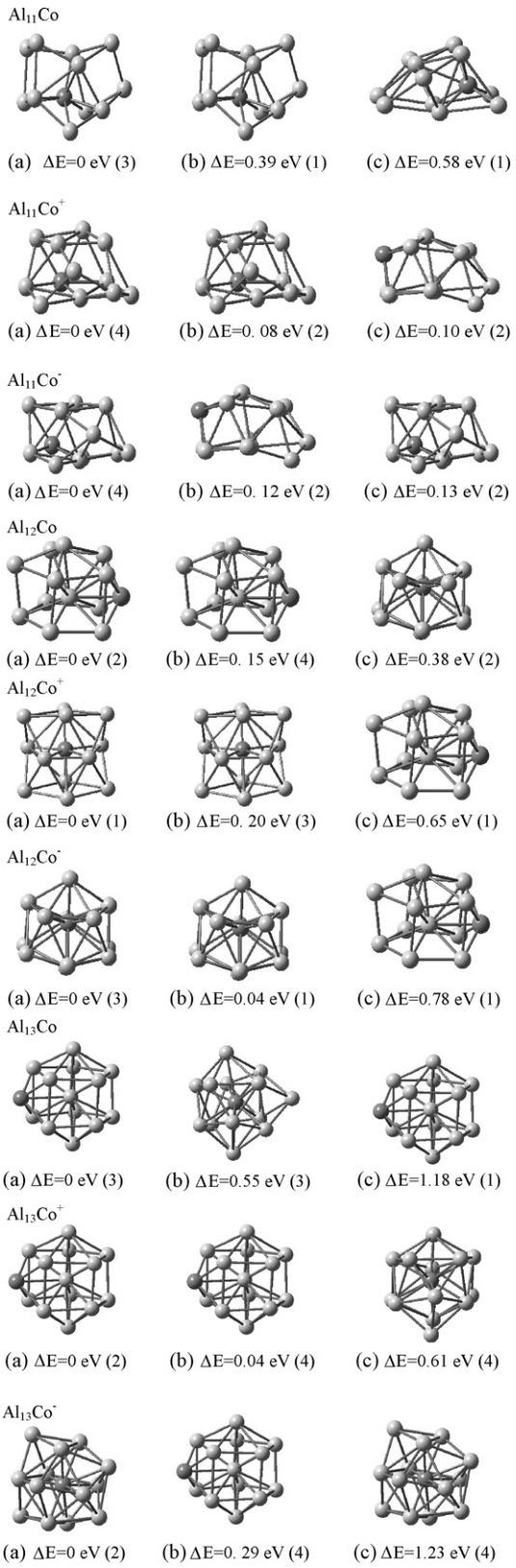

Fig. 1. (*Continued*).

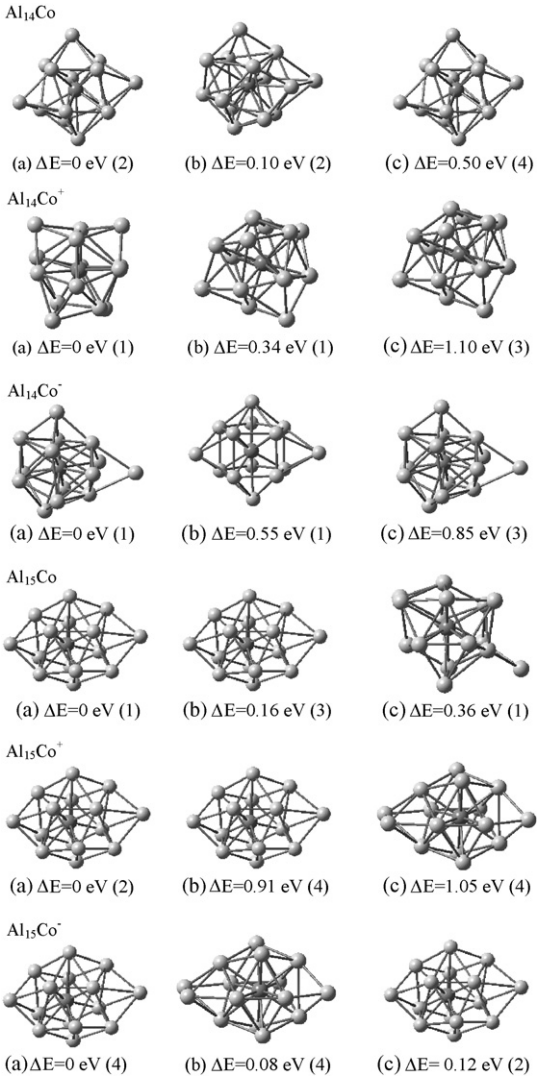

Fig. 1. (*Continued*).

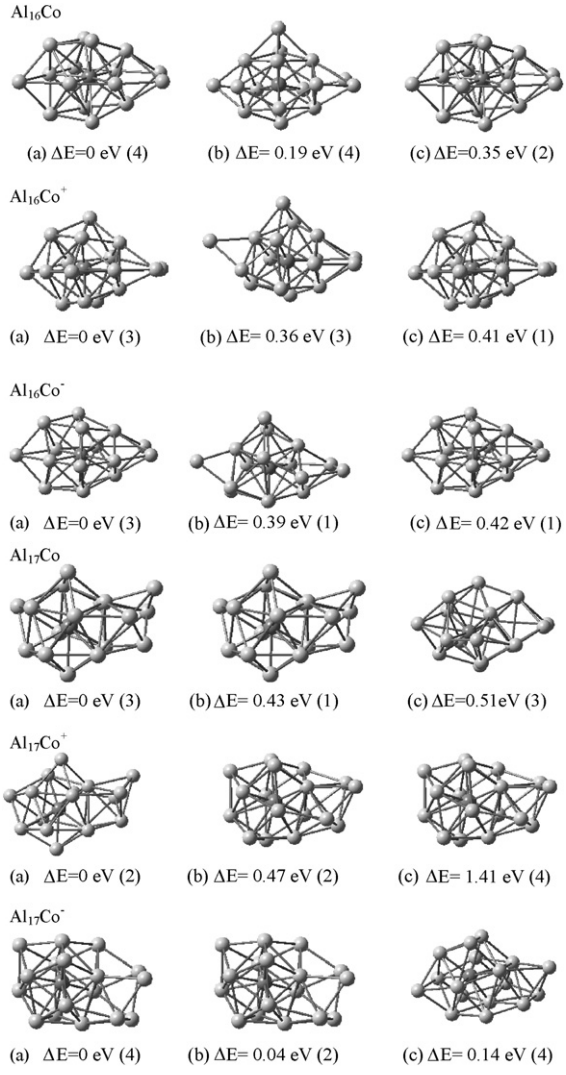

Fig. 1. (*Continued*).

Here R_{ij} is the distance between two atoms i and j with a cut-off = 3.2 Å and n_b is the total number of bonds between atoms that lie below this cutoff. The results are plotted in Fig. 2(a). And the average nearest-neighbor distances in charged clusters computed using Eq. (1) are compared with neutral clusters in Table 2.

3.2. Binding energy and relative stability

The relative stability of clusters can be studied through the measurement of the mass ion intensities and fragmentation channels. However, interpretation of these results is not always unambiguous. Note that in mass spectroscopy experiments, the clusters have to be ionized before their intensities can be mea-

Table 1
Total energies and preferred spin multiplicities of neutral, cationic, and anionic clusters of Al_nCo ($8 \le n \le 17$) in their respective ground-state configurations

n	Neutral E_n (hartree)	Multiplicity	Positive ion E_n^+ (hartree)	Multiplicity	Negative ion E_n^- (hartree)	Multiplicity
8	−161.1700	2	−160.9720	3	−161.2561	1
9	−163.1950	3	−162.9667	2	−163.2753	4
10	−165.1967	2	−164.9791	1	−165.2742	1
11	−167.2148	3	−166.9973	4	−167.3011	4
12	−169.2348	2	−169.0034	1	−169.3265	3
13	−171.2840	3	−171.0527	2	−171.3732	2
14	−173.2948	2	−173.0943	1	−173.3890	1
15	−175.3042	1	−175.0985	2	−175.3913	4
16	−177.3083	4	−177.1022	3	−177.3920	3
17	−179.3289	3	−179.1108	2	−179.4098	4

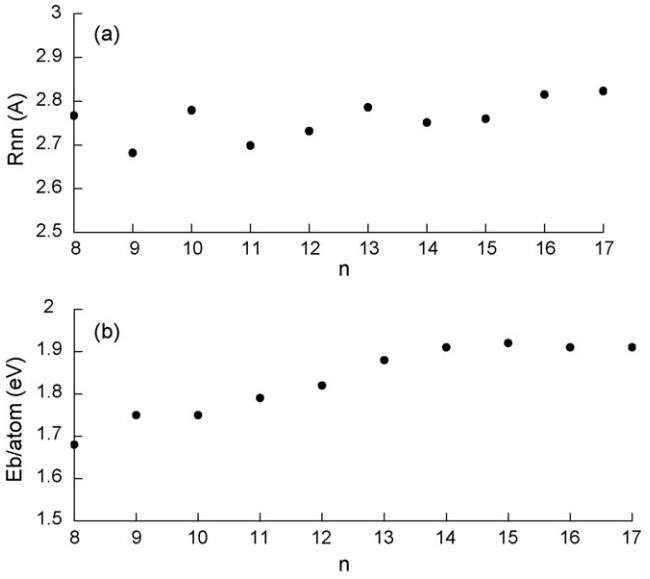

Fig. 2. (a) Average nearest-neighbor distance and (b) binding energy/atom as a function of size for neutral Al_nCo ($n = 8$–17) clusters.

sured. It is not entirely clear if the measured intensity distribution of the clusters represents the stability of the charged clusters or their neutral precursors. For example, if the mass spectra are collected after the ionized clusters have time to relax to their stable configuration, the corresponding mass-ion intensities could be different from the neutral mass distribution.

An unambiguous insight into the relative stability of clusters can be gained by analyzing their energetic. We first compute the binding energy (BE) per atom of the neutral clusters. This is defined by

$$E_b[Al_nCo] = nE[Al] + E[Co] - E[Al_nCo]/n + 1, \quad (2)$$

where $E[Al_nCo]$ is the total energy of the neutral cluster (given in Table 1) and $E[Al](-1.9376$ a.u.) and $E[Co]$ (-145.1134 a.u.) are the energies of the Al and Co atoms, respectively.

The binding energy/atom is E_b is plotted as a function of cluster size in Fig. 2(b). We note that the binding energy rises monotonically with cluster size and contains only a minor bump at $n = 9$ and 16.

To study the relative stability, it is more instructive to analyze the first derivative of the total energy, i.e., the energy gain in adding an atom to an existing cluster. We first investigate this energy gain, hereafter referred to as the stabilization energy, for neutral clusters, namely

$$\Delta E_n^0 = -[E(Al_nCo) - E(Al_{n-1}Co) - E(Al)], \quad (3)$$

These are plotted in Fig. 3(a). Note that one of the factors that contribute to the relative peak heights in the mass spectra of clusters is the magnitude of this energy. There are odd–even alternations from $n = 9$–14, and ΔE_n^0 decreases monotonically from $n = 13$–17. There is a peak at $n = 13$.

We now study the relative stability of the positively charged clusters. In Fig. 3(b) we plot the stabilization energy as an atom is added to an existing positively charged cluster, namely

$$\Delta E_n^+ = -[E(Al_nCo^+) - E(Al_{n-1}Co^+)] - E(Al), \quad (4)$$

where $E(Al_nCo^+)$ corresponds to the total energy of positively charged cluster in its ground state. These energies are given in Table 1. We note that the size dependence of ΔE_n^+ is the same as that seen in Fig. 3(a). For example, there are both odd–even alternations and peak at $n = 13$.

In Fig. 3(c) we plot the stabilization energy in adding an atom to a negative ion cluster, namely

$$\Delta E_n^- = -[E(Al_nCo^-) - E(Al_{n-1}Co^-)] - E(Al), \quad (5)$$

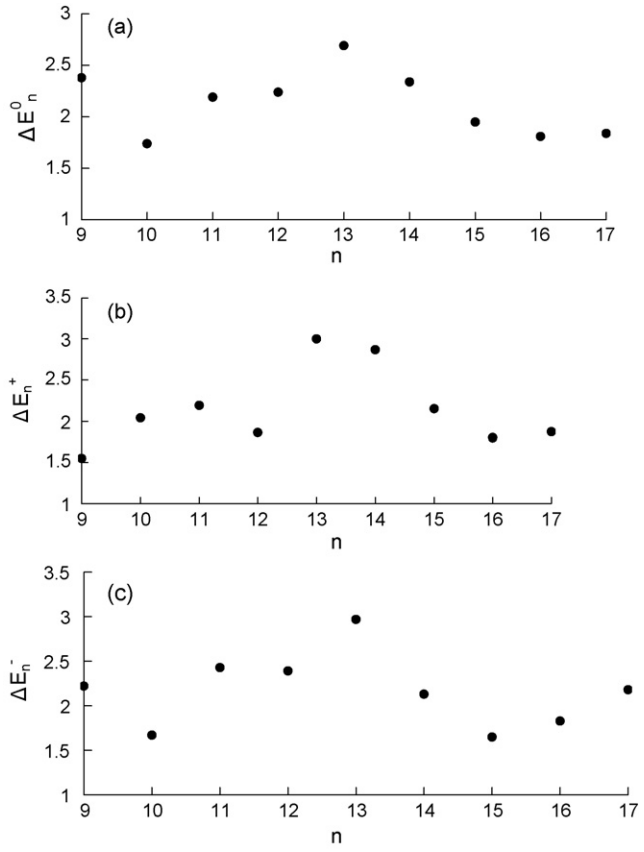

Fig. 3. Energy gain in adding an atom to a (a) neutral cluster, ΔE_n^0, (b) positively charged cluster, ΔE_n^+, and (c) negatively charged cluster, ΔE_n^-, for Al_nCo ($8 \le n \le 17$) clusters.

Table 2
Average nearest-neighbor distances (Å) of neutral, cationic, and anionic cobalt-doped aluminum clusters

n	Neutral	Cation	Anion
8	2.767	2.594	2.590
9	2.682	2.730	2.704
10	2.779	2.692	2.770
11	2.699	2.793	2.797
12	2.732	2.777	2.776
13	2.786	2.786	2.747
14	2.751	2.729	2.763
15	2.760	2.794	2.780
16	2.815	2.807	2.776
17	2.823	2.805	2.788

where $E(Al_nCo^-)$ corresponds to the total energy of the negatively charged n-atom cluster in its ground state. These energies are given in Table 1. We note that the size dependence of ΔE_n^- is similar to that seen in Fig. 3(b) except that the peak corresponding to $Al_{13}Co^-$ is much more pronounced. This is consistent with experimental mass ion intensities [18].

3.3. Electronic structure

The evolution of the electronic structure can be probed by calculating the angular characteristics of the highest molecular orbital (HOMO) as well as the energy gap between HOMO and the lowest unoccupied molecular orbital (LUMO). We have calculated the energy gaps for all the neutral, cationic, and anionic clusters. The results are presented in Figs. 4(a, b and c). Note that a cluster with a closed electronic shell is characterized not only by a large HOMO–LUMO gap but also by a filled HOMO. It also exhibits enhanced binding energy compared to their neighbors. We see from Fig. 4(a) that the HOMO–LUMO gaps in neutral clusters are particularly large for Al_9Co, $Al_{11}Co$, $Al_{13}Co$, and $Al_{15}Co$. We see from Fig. 3(a) that although the energy gain, ΔE_n^0 shows a peak for Al_9Co and $Al_{11}Co$, and a conspicuous peak for $Al_{13}Co$, it has no characteristic feature for $Al_{15}Co$.

The situation is somewhat different for charged clusters. For positively charged Al_nCo clusters (see Fig. 4(b)), the HOMO–LUMO gap exhibit odd–even for $n = 8$–12 with odd-atom clusters having larger HOMO–LUMO gaps than even-atom clusters. For negatively charged Al_nCo clusters (see Fig. 4(c)) conspicuous peak in the HOMO–LUMO gaps exist for $Al_{12}Co^-$ and $Al_{13}Co^-$. We see from Fig. 3(c) that ΔE_n^- for $Al_{13}Co^-$ is large and thus the large HOMO–LUMO gap is consistent with its enhanced stability.

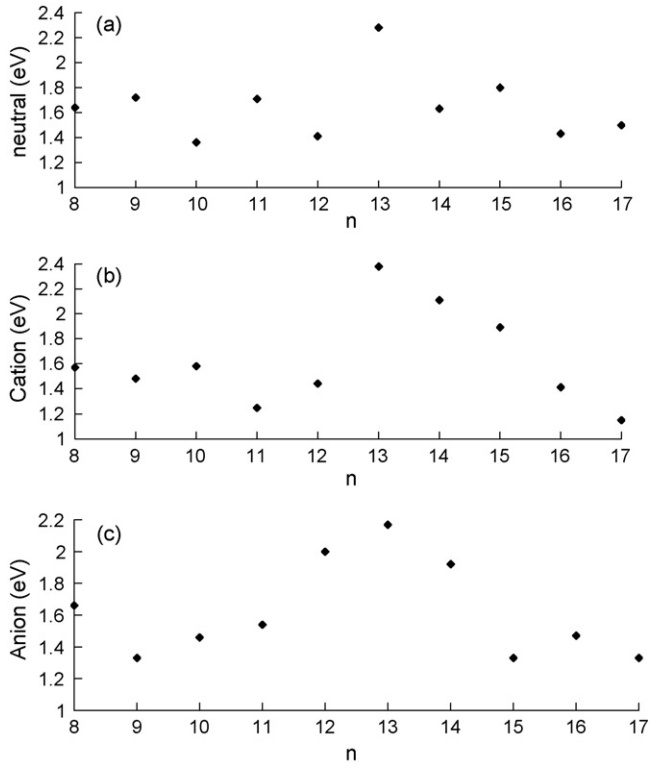

Fig. 4. HOMO–LUMO gaps of (a) neutral, (b) positively charged, and (c) negatively charged Al_nCo ($8 \le n \le 17$) clusters.

3.4. Ionization energy

The ionization energy measures the energy difference between the ground state of the neutral and the ionized clusters, which is another useful quantity for determining the stability of clusters. If the ionized cluster has the same geometry as the ground state of the neutral, the ionization energy corresponds to the vertical ionization potential. On the other hand, the energy difference between the ground state of the cation and ground state of the neutral is referred to as the adiabatic ionization potential. Thus, the vertical ionization energy is always larger than the adiabatic ionization energy and the energy difference between them is an indication of the energy gain due to structural relaxation.

The most detailed experiment of the ionization energies (IE) up to $n = 20$ were carried out by Menezes and co-workers using laser photoionization mass spectrometry. Our calculated ionization energies are in reasonable agreement with experiment. The calculated VIE, AIE and experimental IE values for these clusters are shown in Fig. 5. If the internal temperature of the neutrals is close to absolute zero and the true threshold is identified, photoionization measurements would provide adiabatic ionization energies. If the geometry changes significantly upon ionization, the true threshold would probably not be located, and the measured values would lie between AIE and VIE. As can be seen from Fig. 5, our calculated AIE generally agree reasonable with experimental ionization energies, reproducing all the variations of the IE values especially the global maximum at $Al_{13}Co$ observed in experiments. The calculated VIEs are significantly higher than corresponding AIEs and the measured IEs lie between the calculated AIEs and VIEs in most cases, relatively closer to AIEs. There is one important feature to be noted in Fig. 5. That is, there are no odd–even alternations in the ionization energy as a function of size and there are a conspicuous dip at $n = 15$ and a peak at $n = 13$, which suggest the $Al_{13}Co$

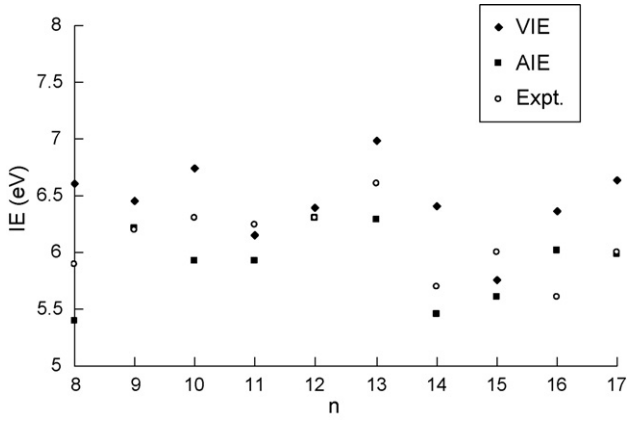

Fig. 5. Comparison of experimental [16] ionization energies (circle) with calculated vertical ionization energy (VIE, rhombus) and adiabatic ionization energy (AIE, square) of Al_nCo ($8 \le n \le 17$) clusters.

Table 3
Adiabatic and vertical electron affinities (AEA, VEA), vertical attachment energies (VAE), adiabatic and vertical ionization energies (AIE, VIE), and HOMO–LUMO gaps of Al_nCo ($8 \le n \le 17$)[a]

n	AEA (eV)		VEA (eV)		VAE (eV)	VIE (eV)	AIE (eV)	HOMO–LUMO gap (eV)
	Theoretical	Experimental	Theoretical	Experimental				
8	2.34	2.00 (20)	2.19	2.67 (13)	1.19	6.60	5.39	1.64
9	2.19	1.82 (18)	2.37	2.38 (11)	2.01	6.46	6.21	1.72
10	2.11	1.93 (19)	2.65	2.59 (12)	1.40	6.75	5.92	1.36
11	2.35	2.05 (20)	3.14	3.12 (15)	1.95	6.15	5.92	1.71
12	2.49	2.15 (21)	3.15	3.13 (15)	1.13	6.39	6.30	1.41
13	2.43	1.66 (16)	3.19	2.91 (14)	1.80	6.99	6.29	2.28
14	2.56	1.96 (19)	3.05	3.15 (15)	2.18	6.41	5.46	1.63
15	2.37	1.83 (18)	3.53	3.25 (16)	2.20	5.76	5.60	1.80
16	2.28	1.77 (17)	2.81	2.40 (12)	2.24	6.36	5.61	1.43
17	2.20	1.65 (16)	2.74	2.25 (11)	2.52	6.63	5.93	1.50

[a] Numbers in parentheses indicate uncertainties of the last digits; 2.00 (20) eV represents 2.00 ± 0.20 eV.

cluster to be the most stable one. This is in with the findings from HOMO–LUMO gap and ΔE_n^0.

3.5. Electron affinities

We next discuss the electron detachment from negatively charged clusters. Here, a size selected negative ion cluster is crossed with a fixed frequency laser and the photodetached electron is energy analyzed. From this, one can measure the binding energy of the electron in the negative ion cluster. The latest work in this series is due to Pramann et al. [18] who studied photoelectron spectroscopy of Al_nCo^- ($n = 8$–17) at 3.49 eV photo energy. Before we discuss our result, we should emphasize that what the experiment actually measures is the difference between the total energy of the ground state of the anion and the total energy of the ground state of the neutral as well as its electronically and vibrationally excited states. Very often the experimental PES spectrum is used to comment on the evolution of the electron density of states of the neutral clusters. There are difficulties associated with the quantitative meaning of this interpretation. First, it relies on the validity of the Koopman's theorem for clusters. Secondly, in density-functional calculations the energy levels have no fundamental meaning. In addition, if the anions contain energetically degenerate isomers, the interpretation of the experimental data becomes further complicated. In our discussion of the electron detachment, we use the total energies of the anionic and neutral clusters.

The photo detachment spectra normally provide two different energies—the vertical and adiabatic electron affinity. The vertical electron affinity (VEA, also called vertical detachment VDE) is the difference in the energy between the ground state of the anion and the energy of the neutral cluster having the anionic geometry. The adiabatic electron affinity (AEA), on the other hand, is the difference in the total energy between the ground state of the anion and the neutral cluster. The vertical attachment energy (VAE) has also been computed, defined as the energy difference between the neutral and anionic clusters with both at the neutral cluster optimized geometry. Although the vertical attachment energy is not currently measure through any experiment, it provides a lower bound to the AEA in the same way, as the VDE is an upper bound to it. The calculated values of the above quantities for the Al_nCo cluster are displayed in Table 3. The relative ordering of the VEA, AEA, and VAE is as expected. And there are odd–even alternations in the VAE as a function of size. In Table 3, we also compare the calculated VEA and AEA with data from Pramann's experiment [18]. We note that the agreement between theory and experiment is reasonable.

4. Conclusions

Using density-functional theory, we have calculated the ground-state geometries of neutral, positively charged, and negatively charged cobalt-doped aluminum clusters Al_nCo ($n = 8$–17). The evolution of the binding energy, atomic and electronic structure, ionization energies, and electron affinities are calculated and compared with experiment. The size of the cobalt atom is smaller than that of aluminum, the ionization energy of Co is high, and the Co atom then occupies an interior site except for $Al_{12}Co$, $Al_{13}Co$, $Al_{11}Co^-$, $Al_{11}Co^+$ and $Al_{13}Co^+$ clusters. And there is considerable mixing between the electronic states of Co and Al. This leads to a strange situation in Al_nCo clusters. And the binding energy also rises monotonically with cluster size and contains only a minor bump at $n = 9$ and 16. Our calculated AIE generally agree reasonable with experimental ionization energies, especially the global maximum at $Al_{13}Co$. By comparing the calculated VEA and AEA with data from Pramann's experiment [18], we find that the agreement between theory and experiment is reasonable.

Acknowledgments

This work was financially supported by the National Natural Science Foundation of China (Grant no. 20603021), Youth Foundation of Shanxi (2007021009) and the Youth Academic Leader of Shanxi.

References

[1] J.H. Sinfelt, J. Catal. 29 (1973) 308.
[2] J.H. Sinfelt, Acc. Chem. Res. 10 (1977) 15.

[3] J.H. Sinfelt, Bimetallic Catalysis: Discoveries, Concepts and Applications, Wiley, New York, 1983.
[4] H.P. Bonzel, Surf. Sci. Rep. 8 (1987) 43.
[5] D.M. Zehner, D.M. Goodman (Eds.), Physical and Chemical Properties of Thin Metal Overlayers and Alloy Surfaces, Mater. Res. Soc. 83 (1987).
[6] X. Li, H. Wu, X. Wang, L. Wang, Phys. Rev. Lett. 81 (1998) 1909.
[7] G.C. Bond, Heterogeneous Catalysis, 2nd ed., Clarendon, Oxford, 1987.
[8] Y. Yamada, A.W. Castleman Jr., J. Chem. Phys. 97 (1992) 4543.
[9] M.P. Andrews, S.C. O'Brien, J. Phys. Chem. 96 (1992) 8233.
[10] M. Heinebrodt, N. Malinowski, F. Tast, W. Branz, I.M.L. Billas, T.P. Martin, J. Chem. Phys. 110 (1999) 9915.
[11] J.M. Behm, M.D. Morse, J. Chem. Phys. 101 (1994) 6500.
[12] Z. Fu, L.M. Russon, M.D. Morse, P.B. Armentrout, Int. J. Mass. Spectrom. 204 (2001) 143.
[13] S. Nonose, Y. Sone, K. Onodera, S. Sudo, K. Kaya, Chem. Phys. Lett. 164 (1989) 427.
[14] B.E. Koel, G.A. Somorjai, in: J.R. Anderson, M. Boudart (Eds.), Catalysis, 7, Springer-Verlag, Berlin, 1985, p. 3.
[15] W.J.C. Menezes, M.B. Knickelbein, Chem. Phys. Lett. 183 (1991) 357.
[16] W.J.C. Menezes, M.B. Knickelbein, Z. Phys. D: Atmos. Mol. Clust. 26 (1993) 322.
[17] J.M. Behm, D.J. Brugh, M.D. Morse, J. Chem. Phys. 101 (1994) 6487.
[18] A. Pramann, A. Nakajima, K. Kaya, J. Chem. Phys. 115 (2001) 5404.
[19] B.K. Rao, P. Jena, J. Chem. Phys. 113 (2000) 1508.
[20] W. Kohn, L.J. Sham, Phys. Rev. 140 (1965) 1133.
[21] R.G. Parr, W. Yang, Density Functional Theory of Atoms and Molecules, Oxford University Press, Oxford, 1989.
[22] W.J. Stevens, H. Basch, M. Krauss, J. Chem. Phys. 81 (1984) 6026.
[23] W.J. Stevens, M. Krauss, H. Basch, P.G. Jasien, Can. J. Chem. 70 (1992) 612.
[24] T.J. Cundari, W.J. Stevens, J. Chem. Phys. 98 (1993) 5555.
[25] A.D. Becke, Phys. Rev. A 38 (1988) 3098.
[26] S.H. Vosko, L. Vilk, M. Nusair, Can. J. Phys. 58 (1980) 1200.
[27] C. Lee, W. Yang, R.G. Parr, Phys. Rev. B 37 (1988) 785.
[28] C.E. Scuseria, J. Chem. Phys. 97 (1992) 7528.
[29] C. Sosa, C. Lee, J. Chem. Phys. 98 (1993) 8004.
[30] M.J. Frisch, G.W. Trucks, H.B. Schlegel, G.E. Scuseria, M.A. Robb, J.R. Cheeseman, V.G. Zakrzewski, J.A. Montgomery Jr., R.E. Stratmann, J.C. Burant, S. Dapprich, J.M. Millam, A.D. Daniels, K.N. Kudin, M.C. Strain, O. Farkas, J. Tomasi, V. Barone, M. Cossi, R. Cammi, B. Mennucci, C. Pomelli, C. Adamo, S. Clifford, J. Ochterski, G.A. Petersson, P.Y. Ayala, Q. Cui, K. Morokuma, D.K. Malick, A.D. Rabuck, K. Raghavachari, J.B. Foresman, J. Cioslowski, J.V. Ortiz, B.B. Stefanov, G. Liu, A. Liashenko, P. Piskorz, I. Komaromi, R. Gomperts, R.L. Martin, D.J. Fox, T. Keith, M.A. Al-Laham, C.Y. Peng, A. Nanayakkara, C. Gonzalez, M. Challacombe, P.M.W. Gill, B. Johnson, W. Chen, M.W. Wong, J.L. Andres, C. Gonzalez, M. Head-Gordon, E.S. Replogle, J.A. Pople, computer code Gaussian 03, Revision B.05, Gaussian, Inc., Pittsburgh PA, 2003.
[31] E.K. Parks, L. Zhu, J. Ho, S.J. Riley, J. Chem. Phys. 100 (1994) 7206, 102 (1995) 7377; S.K. Nayak, S.N. Khanna, B.K. Rao, P. Jena, J. Phys. Chem. 101 (1997) 1072.
[32] E.C. Honea, A. Ogura, C.A. Murray, K. Raghavachari, W.O. Sprenger, M.F. Jarrold, W.L. Brown, Nature (London) 366 (1993) 42.